Carbon 199 (2022) 415–423

Contents lists available at ScienceDirect

Carbon

journal homepage: www.elsevier.com/locate/carbon

Nitrogen implantation into graphene oxide and reduced graphene oxides using radio frequency plasma treatment in microscale

Imre Bertóti [a], Shereen Farah [b], Anna Bulátkó [b], Attila Farkas [c], János Madarász [d], Miklós Mohai [a], György Sáfrán [e], Krisztina László [b,*]

[a] Institute of Materials and Environmental Chemistry, Research Centre for Natural Sciences, Eötvös Loránd Research Network, Budapest, Hungary
[b] Department of Physical Chemistry and Materials Science, Budapest University of Technology and Economics, Budapest, Hungary
[c] Department of Organic Chemistry and Technology, Budapest University of Technology and Economics, Budapest, Hungary
[d] Department of Inorganic and Analytical Chemistry, Budapest University of Technology and Economics, Budapest, Hungary
[e] Research Institute for Technical Physics and Materials Science, Eötvös Loránd Research Network, Budapest, Hungary

ARTICLE INFO

Keywords:
Graphene oxide (GO)
Reduced GO
Plasma treatment
Ambient temperature
Surface modification
X-ray photoelectron spectroscopy (XPS)
Stability

ABSTRACT

Solvent-free radiofrequency (RF) nitrogen plasma treatment was applied to incorporate nitrogen atoms in relatively high concentration. Graphene oxide (GO) and two reduced GOs of different O-content were used as target substrates to reveal the influence of the functional groups decorating the graphene lattice on the quantity and quality of nitrogen incorporation. Despite the relatively high oxygen content of the samples no N–O bonds develop but three kinds of different N–C bonds of very similar concentration are formed. Reduction of the GO removed the O-groups but did not heal the vacancies where N doping may occur. After two days the implanted N content drops, the N1 state (sp^2 N in pyridine ring, C–N–C) showing the least stability.

1. Introduction

Crystalline carbon materials, including carbon nanotubes, graphene and their derivatives, have been in the focus of intensive studies due to their unique structural, physical and chemical properties. They are promising candidates for a wide variety of applications, e.g. within the fields of energy storage and conversion [1–3], supercapacitors or catalyst supports in fuel cells [4,5].

Experimental and theoretical studies showed that nitrogen doping can modulate the band structure of graphene and lead to a metal – semiconductor transition [6–8] and it was also demonstrated that nitrogen doping effectively improved both the microstructure and electrochemical properties of carbonaceous materials [9,10]. The quality, the quantity and the distribution of the nitrogen atoms are crucial for the prospective applications. So far, the usually discussed species for the direct functionalization of carbon materials with nitrogen are pyridinic, pyrrolic and graphitic nitrogen sites within the graphene lattice [9,11]. Beside the deconvolution of the N1s peak by Mueller and his group resulted in an additional signal at 399.3 eV which they assigned to amide, amine and nitrile groups [12]. Nitrogen functionalization and incorporation has been demonstrated by wet chemical methods [13], arc discharge [14], chemical vapor deposition (CVD) [15–17] thermal or electrical annealing [10,11,18–21]. Plasma treatment processes, due to their high efficiency have drawn extensive attention in the reactive modification of graphene materials including oxidation of graphene, reduction of GOs or heteroatom implantation in both types [22–26]. Radio frequency (RF) cold plasma activation is a simple method for fostering gas–solid reactions. The surface activation creates reactive defect-sites or implant the concomitantly excited/ionised gas phase reactants into the sub-surface atomic layers, accommodating them in interstitial, substitutional lattice sites or in vacancies. Practically no environmental hazard arises owing to low energy and reactant consumption, and essentially no emission of harmful by-products occurs. Recent reviews on the synthesis of nitrogen doped graphene or graphene oxide [27,28] concluded that the efficiency of plasma treatment in nitrogen doping noticeably exceeds other methods. Microwave and radiofrequency plasma treatment of graphene or graphene oxide in the presence of N_2 or NH_3 has been reported as an efficient means of introducing nitrogen atom heterogeneities into the graphene layer(s) [5,18–21,29–37]. The amount of incorporated nitrogen varies from technique to technique. It was found that the use of chemical routes does not allow the distribution of N to be localized on the surface [28]. Samples

* Corresponding author.
E-mail address: laszlo.krisztina@vbk.bme.hu (K. László).

https://doi.org/10.1016/j.carbon.2022.08.024
Received 27 May 2022; Received in revised form 1 August 2022; Accepted 3 August 2022
Available online 11 August 2022

prepared by CVD contain segregated domains of nitrogen dopants in the same sublattice [38,39].

Bertóti et al. applied radio frequency (RF) activated N_2 plasma for covalent attachment of nitrogen to different carbon materials, e.g., carbon nanotubes, graphene and graphene oxide [35–37]. By plasma treatment even 8–10% N content [5,31,37] is reachable according to the applied parameters. The method is solvent-free, thereby minimizing re-aggregation of the 2D flakes. The temperature and the duration of the treatment as well as the negative bias occasionally applied allow for further fine tuning of the nitrogen content [12,36,40].

According to Wang et al. higher defect density in the starting material allows for higher N-doping [41,42]. The presence of oxygen containing functional groups on the graphene lattice increases the defect density, this way providing a good starting point for N-doping methods. Moreover, among the several routes which have been published for graphene production, the oxidative exfoliation of graphite is one of the most widely used, cost-effective way. The graphene oxide (GO) obtained then may be reduced or chemically modified to have chemically doped graphene sheets. In spite of the high number of papers published in this field, the effect of the oxygen content on the nitrogen doping possibilities has not been investigated so far. Therefore, one of the goals of the work reported herein was to experimentally study the influence of oxygen functionalities on nitrogen incorporation during the RF plasma treatment of well characterized GO having various O content.

Nitrogen plasma treatment is able to incorporate nitrogen atoms in relatively high concentration, however, the role of the already existing functional groups in this process is hardly known. Our aim was to reveal how the oxygen containing functional groups decorating the graphene lattice influence the quantity and quality of the nitrogen incorporation. Therefore, the radiofrequency plasma treatment was performed on various GO targets having different O-content. The results of the *in-situ* XPS analysis are reported here.

2. Experimental

2.1. Materials

The light brown graphene oxide suspension of 1 w/w% was obtained from natural graphite (GR, Graphite Týn, Týn nad Vltavou, Czech Republic; average particle size 0.063 mm, purity 99.5%) by an improved Hummers' method [43]. Freeze dried GO (GOL) was further treated i) in ambient air at 110 °C yielding sample GO110 and ii) at 300 °C in high purity argon (T45, Linde, Hungary) flow resulting the thermally reduced graphene oxide sample (TRGO). The chemically reduced GO (CRGO) was prepared from the aqueous suspension by applying aqueous ascorbic acid (AA, Molar Chemicals Ltd., Hungary) in the presence of cc NH_4OH (32%, Merck, Hungary) at 368 K for 1 h [44]. Fig. 1 summarizes the sample preparation and the acronym of the samples.

2.2. Plasma treatment

Plasma treatment was performed in the stainless steel sample preparation chamber of the XPS instrument (base pressure $<10^{-4}$ Pa) at room temperature. The high purity N_2 flow of a few mL/min (STP) was regulated by a bleeding valve that set the pressure to 3×10^{-1} Pa. Constant RF power of 100 W at 13.56 MHz was applied through a matching circuit to a coil set outside of a glass dome fixed to the chamber. The sample bias was set to negative value of 300 V (equivalent to 150 eV N ion energy). Following preliminary experiments the treatment time selected was 10 min. After treatment the sample was transferred to the analysis chamber without exposing it to the ambient air.

2.3. Characterization methods

The high resolution images of the samples were taken by a FEI Titan Themis 200 kV spherical aberration (Cs) corrected TEM 0.09 nm HRTEM and 0.16 nm STEM resolution equipped with 4 Thermofischer "Super X G1" EDS detectors. The samples were drop-dried on TEM microgrids coated with ultrathin carbon layer. The crystalline structure was investigated by a PANalytical X'Pert Pro MPD X-ray diffractometer using monochromatic Cu Kα radiation (λ = 1.5406 Å) at 40 keV and 30 mA. The results were analyzed by an X'Pert High Score software, applying Bragg's [45] and the Scherrer equation [46] to estimate the lattice spacing d and the mean size of the ordered domains L_c. Raman spectra were measured with a LabRAM (Horiba Jobin Yvon) instrument having a λ = 532 nm Nd-YAG laser source (laser power at the focus point is 15 mW). A 0.6 OD filter was used to reduce the intensity of the excitation beam to suppress the chance of sample degradation. LabSpec 5 software was applied for parameter optimization and data collection. After baseline correction the first and second order regions of the spectra were deconvoluted to Lorentzian peaks using the conventional fitting procedure of the Origin program. The lateral size L_a of the graphenic platelets was estimated by the Tuinstra-Koenig-Cancado equation [47].

$$L_a = (2.4 \times 10^{-10})\, \lambda^4\, (I_D / I_G)^{-1} \quad (1)$$

where λ is the excitation laser wavelength (nm), I_D and I_G are the intensity of D-band and G-band, respectively. The Fourier-transform infrared (FTIR) spectra were collected on Attenuated Total Reflection Fourier Transform Infrared spectrophotometer (ATR-FTIR, Bruker).

X-ray photoelectron spectra were recorded on a Kratos XSAM 800 spectrometer operating in fixed analyzer transmission mode, using Mg $K\alpha_{1,2}$ (1253.6 eV) excitation. The pressure of the analysis chamber was lower than $1 \cdot 10^{-7}$ Pa. Survey spectra were recorded in the kinetic energy range 150–1300 eV in 0.5 eV steps, while photoelectron lines of the main constituent elements (O1s, N1s and C1s) were recorded in 0.1 eV steps with 1 s dwell time. Spectra were referenced to the energy of the C1s line of the sp^2 type graphitic carbon, set at 284.3 ± 0.1 eV binding energy (BE). Peak decomposition was performed after Shirley-type background removal using Gaussian–Lorentzian peak shape with

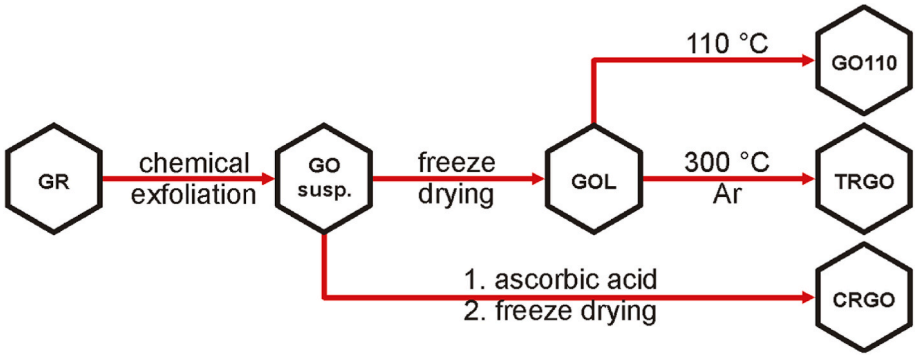

Fig. 1. Preparation and acronyms of the samples.

70:30 ratio. Details of the applied fitting procedure is described elsewhere [37].

Quantitative analysis, based on integrated peak intensity, was performed by the XPS MultiQuant program [48,49], applying the conventional infinitely thick layer model using the experimentally determined photoionisation cross-section data of Evans et al. [50] and the asymmetry parameters of Reilman et al. [51].

3. Results and discussion

3.1. Characterization of the samples

The alteration of the graphitic order during the wet chemical exfoliation and the following reductions is reflected by both the TEM images (Fig. 2), the XRD patterns and the Raman spectra in Fig. 3. The main structural parameters deduced from XRD and Raman spectroscopy are shown in Table S1.

For GO derivatives Raman spectroscopy and XRD act as complementary tools to characterize the morphology of the samples [52]. The deconvolution of the Raman spectra allows not only the assignment of the emblematic G (ca 1580 cm^{-1}, graphitic band, related to the vibrations of the sp^2 building blocks) and D (ca 1350 cm^{-1}, defect band, associated to structural disorder) bands but also the contribution of D' (ca 1600 cm^{-1}, disordered graphitic lattices), D" (ca 1506 cm^{-1}, amorphous phases) and D* (ca 1220 cm^{-1}, disorder from graphitic lattices and impurities) in the first order spectrum [53–55]. In the second order spectrum, beside the 2D band (ca 2700 cm^{-1}, structural order), G*, D + D′ and 2D' bands contributing to the 2300 - 3100 cm^{-1} region were identified [56,57]. The iconic I_D/I_G ratio (0.17 in the parent graphite) dramatically increased after the oxidative exfoliation indicating a high degree of disorder. The decrease in the extension of the in-plane sp^2 domains seems to be more expressed during the chemical treatment. The G and 2D bands usually appearing at 1585 and 2679 cm^{-1} in single layer graphene are shifted here to lower and higher values, respectively, showing that on average all the samples contain more than a single layer which is also confirmed by the low I_{2D}/I_G ratio (>1.6 in single layer graphene) and agrees with the XRD results [58–60]. The L_a and L_c values in GR were 113 and 40 nm, respectively. The wet exfoliation led to a significant fragmentation, more severely in the lateral dimension, which on the other hand, was hardly affected by the reductive treatments. Eq. (1), however, should be applied with caution, as the value of L_a is defined by the Raman active defects than by the "physical" extension of the platelets [61].

The XRD and Raman results unanimously confirm a delicate morphological difference between the thermal and chemical treatments applied here. The latter one results in platelets with narrower interlayer distance, smaller lateral dimension and higher I_D/I_G ratio.

The ATR-FTIR spectrum of the GOL sample is very rich in signals from O-containing functional groups (Fig. S1). The broad and intense band in the 3000-3700 cm^{-1} corresponds to the O–H stretching vibrations. The narrow bands at about 1740 cm^{-1} and in the 1570-1620 cm^{-1} range mark the C═O stretching vibrations from carbonyl and carboxyl groups and the C═C skeletal vibrations of O-free graphitic domains, respectively. The deformation shoulder at 1384 cm^{-1} belongs to the O–H bending vibrations of hydroxyl groups, while the bands within 1010–1215 cm^{-1} can be attributed to epoxy, ether or peroxide functionalities [62,63]. The difference between the TRGO and CRGO spectra reflects again the different efficiency of the applied physical and chemical reduction treatments. While all the features marking O-containing functional groups are below the detection limit in the CRGO sample TRGO still possesses some of the functional groups within the 900-1800 cm^{-1} region, although with a reduced intensity. The carboxyl groups certainly decompose at the temperature of the heat treatment, but the carbonyl stretching vibrational peak is still present in TRGO. This implies that the more stable ketones or conjugated quinones might be retained in the bulk sample [64].

XPS analysis performed prior to the plasma treatment approve the observations above. Although XPS is a surface analytical method, in case of 2D nanoparticles its information depth is close to the thickness of the particles. The total surface compositions based on the "infinitely thick homogeneous sample" model, are shown in Table 1.

The surface composition of the GOL sample was identical to that of the GO110 sample, revealing that the 5% water detected by TG/DTG analysis was removed during the high-vacuum treatment in the XPS sample preparation chamber. An additional evidence was the lack of signal at BE~536 eV [65].

The considerable oxygen content of the GO110 sample significantly decreased during both reductive steps (TRGO, CRGO) explaining the constricted interlayer distance. The chemical reduction was more efficient, as shown by the O/C ratio, also confirmed by the FTIR results. On the other hand, it also led to more fragmented graphene like platelets according to the Raman results. The source of the small amount of nitrogen in the CRGO is related to the presence of NH_3 in the reaction medium. The shape of the O1s, N1s and C1s photoelectron lines of the samples are compared in Fig. 4 (upper row). The high oxygen content of the GO110 sample is clearly reflected by the C1s line shape (in GO samples with high oxygen content the asymmetry of the C1s peak is less obvious), while the shape of the reduced samples is almost identical.

All complex lines could be decomposed by a similar scheme (same components with varying intensity), as illustrated by the GO110 sample in Fig. 5 (upper row). Assignation of components to chemical states are based on our previous results and on literature data [66,67] and enumerated in Table 2. The oxygen balance (Table S2), the ratio of the measured and calculated (required by the other elements) oxygen content, is fairly close to 1 (±10%), which also supports the assignation of chemical states.

During the reduction the surface concentration of all oxygen components decreased, most spectacularly the O2 (C–O–C, C–OH) and O1

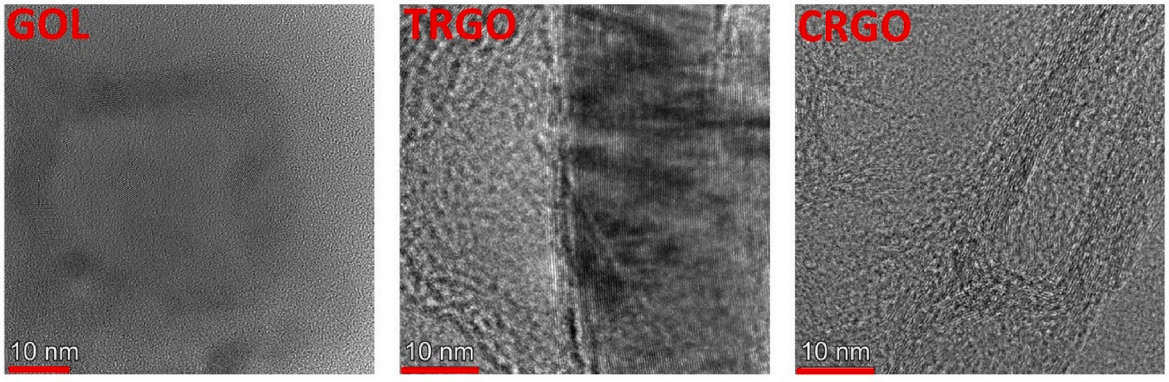

Fig. 2. TEM image of the GOL, TRGO and CRGO samples. The scale bar is 10 nm. (A colour version of this figure can be viewed online.)

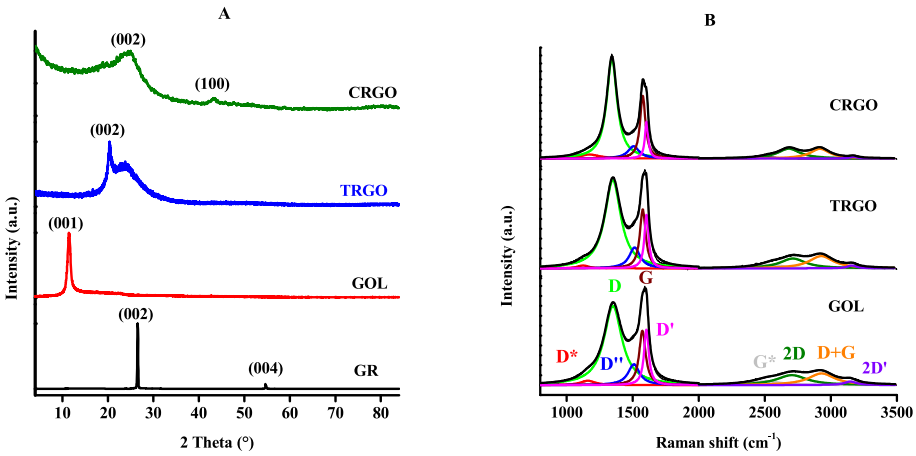

Fig. 3. Powder X-ray diffractograms (A) and the Raman spectra (B) of the samples prior to plasma treatment. The normalized graphs are vertically shifted. (A colour version of this figure can be viewed online.)

Table 1
The overall surface compositions (atomic %) of the untreated and nitrogen plasma treated samples, calculated by the "infinitely thick homogeneous sample" model.

Sample		C	O	N	O/C	N/C	(O + N)/C
pristine	GO110	75.1	24.9	0.0	0.33	–	0.33
	TRGO	85.2	14.9	0.0	0.17	–	0.17
	CRGO	87.1	9.9	3.0	0.11	0.03	0.15
plasma treated	GO110 N	72.0	12.4	15.6	0.17	0.22	0.39
	TRGON	76.0	8.3	15.7	0.11	0.21	0.32
	CRGON	73.2	10.0	16.9	0.14	0.23	0.37

components as reflected by the change of the O1s line shape in Fig. 5 and the corresponding concentrations in Fig. 6 and Table S3. Accordingly, the C1 – C4 carbon components also underwent a significant modification.

3.2. *Effect of the plasma treatment*

The efficiency of the radiofrequency plasma treatment applied to introduce N functionalities was followed by XPS. Plasma treated samples are distinguished by an N postfix. The development of the spectra is shown in Figs. 4 and 5, while the C1s, O1s and N1s concentrations are given in Table 1 and Fig. 6.

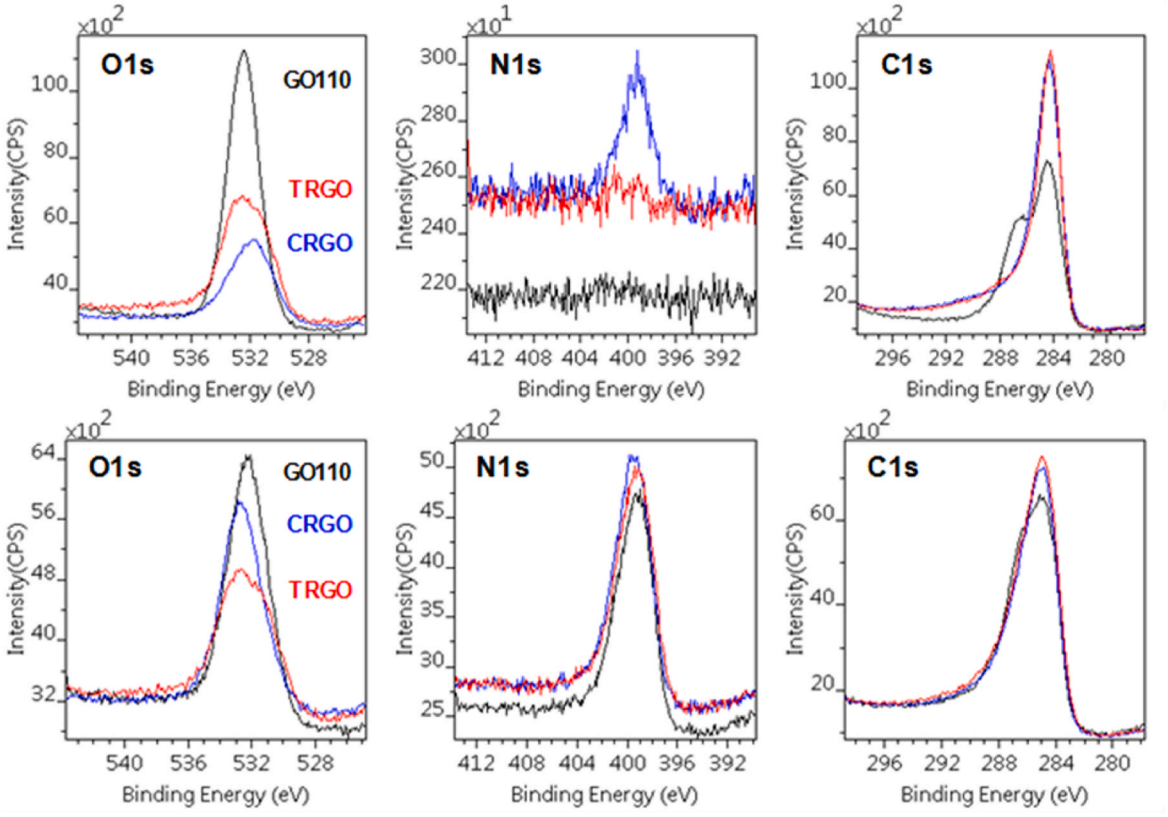

Fig. 4. Comparison of the O1s, N1s and C1s photoelectron lines of the untreated (upper row) and N plasma treated (lower row) samples. (A colour version of this figure can be viewed online.)

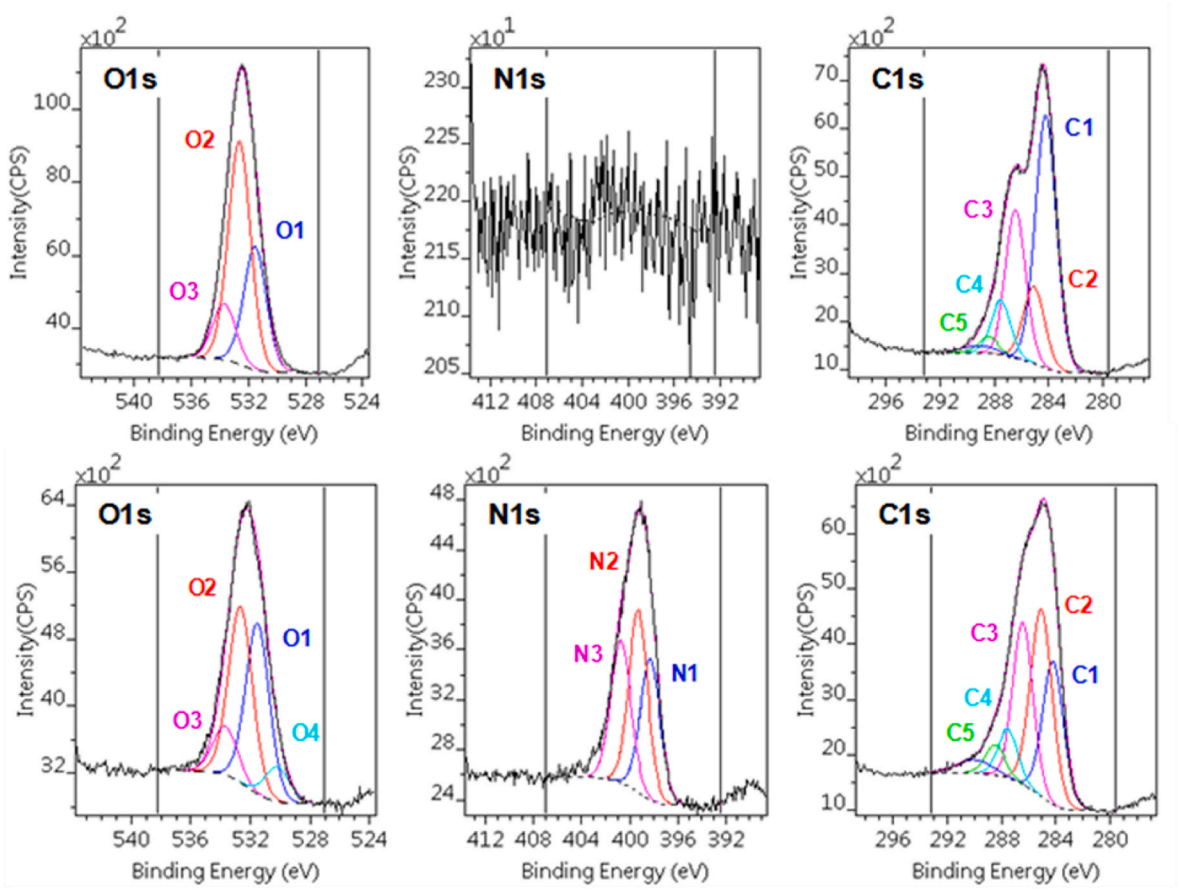

Fig. 5. Typical example of decomposition of the O1s, N1s and C1s photoelectron lines to various chemical sates of the untreated (upper row) and N plasma treated (lower row) GO110 sample. (A colour version of this figure can be viewed online.)

Table 2
Assignation of the chemical states to the various C, O and N[a] components applied to decompose complex photoelectron lines of the nanocarbon materials.

Component	Binding energy (eV)	Chemical states
C1	284.3 ± 0.1	sp^2 C
C2	285.1 ± 0.2	sp^3 C
C3	286.4 ± 0.2	C–O–C, C*–O–C–O, C–OH, C–N
C4	287.7 ± 0.2	C═O, C_3N
C5	288.7 ± 0.2	O═C–O, O═C–N
O1	531.5 ± 0.2	O–C–N, aromatic C═O
O2	532.6 ± 0.2	C–O–C, aliphatic C–OH
O3	533.5 ± 0.2	O*–C═O, H*O–C═O
O4	530.5 ± 0.2	aliphatic C═O, graphene oxide
N1	398.4 ± 0.2	sp^2 N in pyridine ring, C–N–C
N2	399.4 ± 0.2	sp^2 N in pyrrole or diazine ring, C═N, N–C═O
N3	400.5 ± 0.2	N in graphene plane, N–COO, O═C–N–C═O

[a] N species are illustrated in Fig. S2.

The plasma treatments implant a relatively large amount (over 15%) of nitrogen. The penetration depth of the 150 eV N ions into graphene oxide, calculated by the SRIM-2013 program [68], is 3.6 nm, which is approximately the half of the information depth of XPS for this system. Thus the resulted concentrations are representative as average to the whole modified layer. The nitrogen content in the top surface layer may be even higher. Plasma treatment, like other energetic particle treatments, e.g., ion bombardment, reduces the graphene oxide. Nitrogen atoms, being chemically active, are especially effective compared to inactive species, such as Ar [69]. In the case of other nanocarbon materials (graphene, nanotubes, etc.) with limited oxygen content the concentration of the built-in N is lower than that for GO [37] suggesting that the presence of C–O groups promotes N incorporation through oxygen exchange with nitrogen.

The plasma treatment reduced all samples to a comparable oxidation level, the O loss in the GO sample was 50%. In the chemically reduced GO, no significant oxygen loss was observed. In the case of the GO and the thermally reduced samples the loss of O coincided with the N inclusion and the increase of the overall O + N content, particularly in the case of the TRGO sample. Although the O concentration was not affected by the plasma treatment the highest N content was achieved in the CRGO sample, while in the other two samples N was incorporated with similar, but lower efficiency. The similarity of the (O + N)/C atomic ratio in the three plasma treated samples (Table 1) suggests that the final states of the samples are also alike.

The chemical states of C and O constituents of the plasma treated samples are analogous to those of the untreated ones (Fig. 5, lower row). The treatments create three new different N–C bonds (Table 3). Despite the relatively high oxygen content of the untreated samples, N–O bonds did not develop in the conditions employed.

The quantitative relations between the components are shown in Fig. 6 and Table S3. The concentration of the incorporated nitrogen is almost the same for all the three types, and there are only minor differences in oxygen concentrations. The trends observed in the untreated samples suggest that the C3 – O2 (C–O–C, C–OH), the C4 – O1 (C═O) and the C5 – O3 (O–C═O) components are bonded, which is in good agreement with the assigned chemical states. During reduction, decrease occurred mainly in the concentration of C3, moderately of C4, while the quantity of C5 is practically unchanged. As the binding energy ranges of the C–O and C–N bonds overlap, the corresponding chemical states cannot be assigned quantitatively to each of these bonds. Nevertheless,

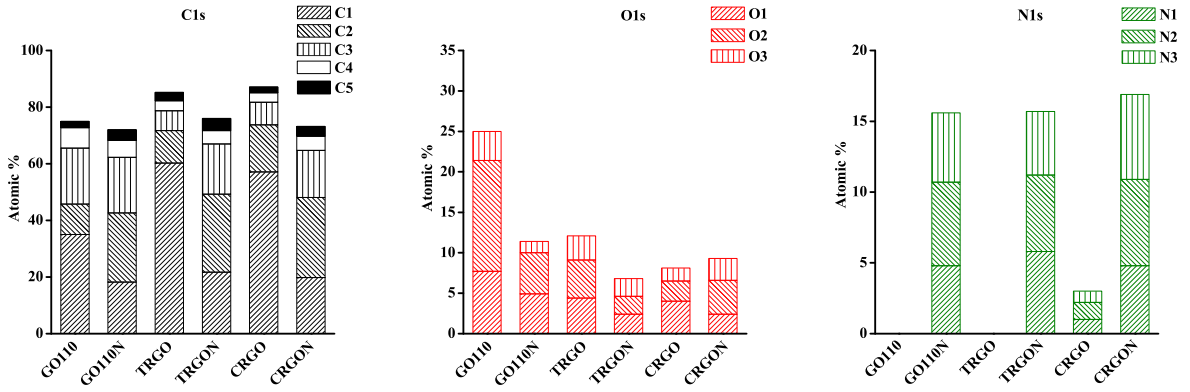

Fig. 6. Distribution of the various C1s, O1s and N1s components before and after the plasma treatment (Numerical data are given in Table S3.). (A colour version of this figure can be viewed online.)

Table 3
Overall surface compositions (atomic %) and atomic ratios of the aged GO110 sample before and after nitrogen plasma treatment and 48 h air exposure.

History of the sample	C	O	N	O/C	N/C	(O + N)/C
GOA	69.9	30.1		0.43		0.43
GOA-N	67.2	24.0	8.8	0.36	0.13	0.49
GOA-NA	68.5	25.2	6.3	0.37	0.09	0.46

the trends show that the C3 – N1, N2; C4 – N3 and C5 – N2, N3 bonds are plausible.

A closer analysis of the surface compositions, however, implies that the assumed correspondence between the initial O content and the final N content has not been confirmed, i.e., the mechanism is more sophisticated than a plain C–O to C–N substitution. After the plasma treatment CRGO with the lowest O content ended up with the highest overall N content while its overall O content was not affected. Moreover, almost 40% of its N content is in N3 state. This sample has a particularly low concentration of O2 and O3 states after the chemical reduction which lead also to the lowest interlayer distance. That indicates that the chemical reduction left behind more vacancies than the thermal treatment in the carbon plane which readily accommodate the N atoms. The alteration of the distribution of the O species also implies the rearrangement of the O states.

3.3. *Persistency of the surface functional groups*

The influence of aging on the GO and the persistency of the N species introduced by the plasma treatment was studied on the GO110 sample by XPS. Two aspects of the atmospheric exposure were tested according to the scheme presented in Fig. 7. The surface compositions of these samples are shown in Tables 3–4 and Fig. 8.

The GO110 sample was stored in air ambient for one year. As expected, during the long-term ambient storage the total oxygen content (Table 3) increased. The concentration of the O1 and O2 oxygens and the corresponding C3 carbon increased, while the concentration of the C1 and C2 species decreased (Table 4). The aged GOA sample was then treated with the nitrogen plasma as previously. The trends of concentration changes during the N plasma treatment of the aged GOA sample are similar to those of the fresh sample but the overall level of the built-in nitrogen is lower. The concentration of the O1 component was not decreased, unlike that of the fresh sample (Fig. 8).

While in the GO110 sample the treatment halved the O content, this effect was much more limited in the aged GOA sample. Interestingly, the change in the overall heteroatom composition is similar in the two treatments resulting in a total (O + N)/C ratio as high as 0.49 in the GOA-N sample. In both the GO110 and the GOA samples the C2 and O2 species alter the most. While the distribution of the N species in the GO110 N sample is relatively even, in GOA-N ca 50% of the N is in N1 state. In order to study the persistency of the freshly introduced N species the GOA-N sample was kept in ambient air for 48 h. Within this short period the O/C ratio does not change, but the N content diminishes, the N1 form seems to be particularly unstable. The corresponding C3 carbon is transformed to C1.

The O heteroatoms are sensitive to the plasma treatment and part of them is removed efficiently. In the graphene oxides the amount of N atoms built in always exceeds the number of removed O atoms implying that already existing or new vacancies are also activated to give rise to N3 type nitrogen states, while in highly ordered purely graphenic structures the nitrogen is incorporated typically in N1 and N2 forms [70]. The role of vacancies is the most obvious during the plasma treatment of the chemically reduced GO sample, (CRGO → CRGON) as the reduction removes part of the oxygen groups but does not remove the vacancies. In GOA sample the oxidation and the redistribution of the O functionalities during the storage resulted in a limited reactivity of the vacant sites and thus a lower overall N and particularly N3 type incorporation.

4. Conclusions

The solvent free radiofrequency plasma treatment was applied on graphene oxide and its reduced derivatives to reveal the influence of the oxygenic functional groups on the nitrogen implantation. Three kinds of different N–C bonds of very similar concentration were formed in all the samples in spite of their different O/C ratio and the different distribution of the O-functionalities present. Despite the relatively high oxygen content of the target samples no N–O bonds develop. However, the presence of C–O groups promotes the N incorporation through oxygen to nitrogen exchange. Reduction of the GO may remove the O-groups but does not heal the vacancies where N doping may happen effectively. After two days the N content drops, the N1 form showing the least

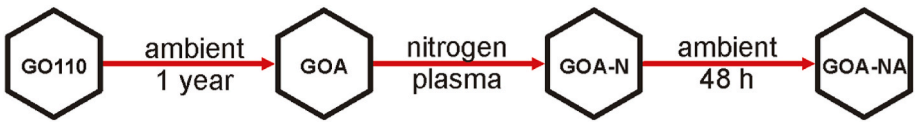

Fig. 7. History and acronyms of the samples for aging study.

Table 4
Changes of the surface compositions (atomic %) of the chemical states of the GO110 sample during long term ageing.

Treatment	C 1	C 2	C 3	C 4	C 5	O 1	O 2	O 3
GO110	35.0	10.8	19.7	7.3	2.2	7.7	13.7	3.6
GOA	24.9	4.2	34.8	4.0	2.0	10.8	17.8	1.6
Difference (%)	−28.9	−61.1	+76.6	−45.2	−9.1	+40.3	+29.9	−55.6

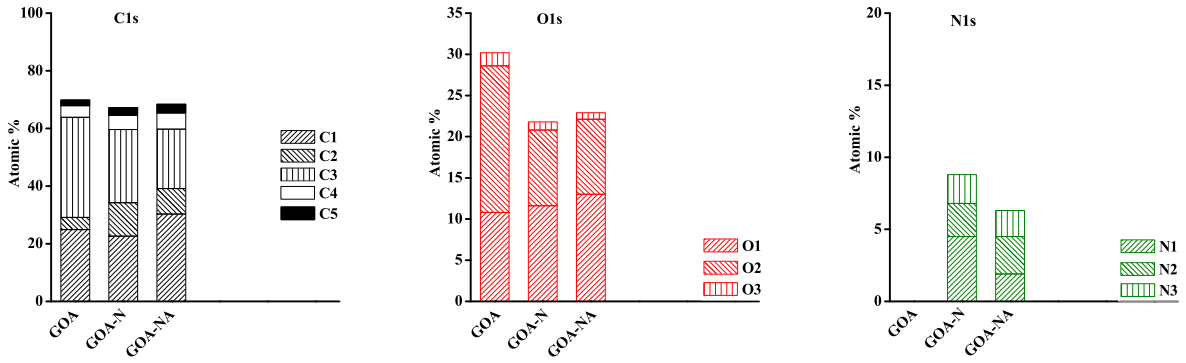

Fig. 8. Distribution of the various C1s, O1s and N1s components in the aged GO110 aged GO110 sample before and after nitrogen plasma treatment and 48 h air exposure (Numerical data are given in Table S4.).

stability.

CRediT authorship contribution statement

Imre Bertóti: Conceptualization. **Shereen Farah:** Investigation, Formal analysis. **Anna Bulátkó:** Data curation. **Attila Farkas:** Investigation, Supervision. **János Madarász:** Investigation, Supervision. **Miklós Mohai:** Methodology, Formal analysis, Writing – original draft, review. **György Sáfrán:** Visualization. **Krisztina László:** Conceptualization, Writing – original draft, Writing – review & editing, Funding acquisition, Project administration.

Declaration of competing interest

The authors declare that they have no known competing financial interests or personal relationships that could have appeared to influence the work reported in this paper.

Acknowledgment

We extend our warm thanks to B. Berke and G. Bosznai for their invaluable assistance. Financial support from the H2020-MSCA-RISE-2016-734641 NanoMed project, the Hungarian Scientific Research Funds OTKA K128410 and VEKOP-2.3.2-16-2017-00013 is acknowledged. The VEKOP project is supported by the EU and by Hungary, co-financed by the European Regional Development. The research reported in this paper is part of project no. BME-NVA-02, implemented with the support provided by the Ministry of Innovation and Technology of Hungary from the National Research, Development and Innovation Fund, financed under the TKP2021 funding scheme. SF is grateful to the Stipendium Hungaricum scholarship program of the Hungarian Government and for the financial support of the Ministry of Higher Education and Research, Sudan as well as University of Khartoum, Sudan.

Appendix A. Supplementary data

Supplementary data to this article can be found online at https://doi.org/10.1016/j.carbon.2022.08.024.

References

[1] H. Wu, W. Lu, J. Shao, C. Zhang, M. Wu, B. Li, Q. Yang, pH-dependent size, surface chemistry and electrochemical properties of graphene oxide, N. Carbon Mater. 28 (2013) 327–335, https://doi.org/10.1016/S1872-5805(13)60085-2.
[2] L. Dai, Functionalization of graphene for efficient energy conversion and storage, Acc. Chem. Res. 46 (2013) 31–42, https://doi.org/10.1021/ar300122m.
[3] Y. Xue, H. Chen, J. Qu, L. Dai, Nitrogen-doped graphene by ball-milling graphite with melamine for energy conversion and storage, 2D Mater. 2 (2015), 044001, https://doi.org/10.1088/2053-1583/2/4/044001.
[4] H. Su, Y.H. Hu, Recent advances in graphene-based materials for fuel cell applications, Energy Sci. Eng. 9 (2021) 958–983, https://doi.org/10.1002/ese3.833.
[5] Y. Shao, S. Zhang, M.H. Engelhard, G. Li, G. Shao, Y. Wang, J. Liu, I.A. Aksay, Y. Lin, Nitrogen-doped graphene and its electrochemical applications, J. Mater. Chem. 20 (2010) 7491–7496, https://doi.org/10.1039/C0JM00782J.
[6] M. Deifallah, P.F. Mcmillan, F. Cora, Electronic and structural properties of two-dimensional carbon nitride graphenes, J. Phys. Chem. C 112 (2008) 5447–5453, https://doi.org/10.1021/jp711483t.
[7] F. Cervantes-Sodi, G. Csányi, S. Piscanec, A.C. Ferrari, Edge-functionalized and substitutionally doped graphene nanoribbons: electronic and spin properties, Phys. Rev. B 77 (2008), 165427, https://doi.org/10.1103/PhysRevB.77.165427.
[8] T.O. Wehling, K.S. Novoselov, S.V. Morozov, E.E. Vdovin, M.I. Katsnelson, A. K. Geim, A.I. Lichtenstein, Molecular doping of graphene, Nano Lett. 8 (2008) 173–177, https://doi.org/10.1021/nl072364w.
[9] H. Terrones, M. Terrones, E. Hernández, N. Grobert, J.-C. Charlier, P.M. Ajayan, New metallic allotropes of planar and tubular carbon, Phys. Rev. Lett. 84 (2000) 1716–1719, https://doi.org/10.1103/PhysRevLett.84.1716.
[10] H. Wang, C. Zhang, L. Wang, P. Han, H. Xu, K. Zhang, S. Dong, J. Yao, G. Cui, Nitrogen-doped graphene nanosheets with excellent lithium storage properties, J. Mater. Chem. 21 (2011) 5430–5434, https://doi.org/10.1039/C1JM00049G.
[11] B. Guo, Q. Liu, E. Chen, H. Zhu, L. Fang, J.R. Gong, Controllable N-doping of graphene, Nano Lett. 10 (2010) 4975–4980, https://doi.org/10.1021/nl103079j.
[12] A. Mueller, M.G. Schwab, N. Encinas, D. Vollmer, H. Sachdev, K. Müllen, Generation of nitrile groups on graphites in a nitrogen RF-plasma discharge, Carbon 84 (84) (2015) 426–433, https://doi.org/10.1016/j.carbon.2014.11.054.
[13] F.M. Koehler, A. Jacobsen, K. Ensslin, C. Stampfer, W.J. Stark, Selective chemical modification of graphene surfaces: distinction between single- and bilayer graphene, Small 6 (2010) 1125–1130, https://doi.org/10.1002/smll.200902370.
[14] L.S. Panchakarla, K.S. Subrahmanyam, S.K. Saha, A. Govindaraj, H. R. Krishnamurthy, U.V. Waghmare, C.N.R. Rao, Synthesis, structure, and properties of boron- and nitrogen-doped graphene, Adv. Mater. 21 (2009) 4726–4730, https://doi.org/10.1002/adma.200901285.
[15] L. Qu, Y. Liu, J.-B. Baek, L. Dai, Nitrogen-doped graphene as efficient metal-free electrocatalysts for oxygen reduction in fuel cells, ACS Nano 4 (2010) 1321–1326, https://doi.org/10.1021/nn901850u.
[16] R. Lv, M. Terrones, Towards new graphene materials: doped graphene sheets and nanoribbons, Mater. Lett. 78 (2012) 209–218, https://doi.org/10.1016/j.matlet.2012.04.033.
[17] A.L.M. Reddy, A. Srivastava, S.R. Gowda, H. Gullapalli, M. Dubey, P.M. Ajayan, Synthesis of nitrogen-doped graphene films for lithium battery application, ACS Nano 4 (2010) 6337–6342, https://doi.org/10.1021/nn101926g.

[18] X. Li, H. Wang, J.T. Robinson, H. Sanchez, G. Diankov, H. Dai, Simultaneous nitrogen doping and reduction of graphene oxide, J. Am. Chem. Soc. 131 (2009) 15939–15944, https://doi.org/10.1021/ja907098f.
[19] X. Wang, X. Li, L. Zhang, Y. Yoon, P.K. Weber, H. Wang, J. Guo, H. Dai, N-doping of graphene through electrothermal reactions with ammonia, Science 324 (2009) 768–771, https://doi.org/10.1126/science.1170335.
[20] C. Wang, J. Kang, H. Sun, H.M. Ang, M.O. Tadé, S. Wang, One-pot synthesis of N-doped graphene for metal-free advanced oxidation processes, Carbon 102 (2016) 279–287, https://doi.org/10.1016/j.carbon.2016.02.048.
[21] S. Yang, L. Zhi, K. Tang, X. Feng, J. Maier, K. Müllen, Efficient synthesis of heteroatom (N or S)-doped graphene based on ultrathin graphene oxide-porous silica sheets for oxygen reduction reactions, Adv. Funct. Mater. 22 (2012) 3634–3640, https://doi.org/10.1002/adfm.201200186.
[22] B. Tincu, M. Avram, A. Avram, V. Tucureanu, G. Mihai, M. Popa, P. Osiceanu, I. Demetrescu, M. Enachescu, Investigation of plasma-assisted functionalization of pristine single layer graphene, Chem. Phys. Lett. 789 (2022), 139330, https://doi.org/10.1016/j.cplett.2021.139330.
[23] F.M. El-Hossary, Ghitas Ahmed, A.M. Abd El-Rahman, A.A. Ebnalwaled, M. Abdelhamid Shahat, M.H. Fawey, Cold RF oxygen plasma treatment of graphene oxide films, J. Mater. Sci. Mater. Electron. 32 (2021) 15718–15731, https://doi.org/10.1007/s10854-021-06123-x.
[24] F.K. Alosaimi, T.T. Tung, V.-D. Dao, N.K. Huyen, M.J. Nine, K. Hassan, J. Ma, D. Losic, Graphene-based multifunctional surface and structure gradients engineered by atmospheric plasma, Appl. Mater. Today 27 (2022), 101486, https://doi.org/10.1016/j.apmt.2022.101486.
[25] N.S. Singh, F. Mayanglambam, H.B. Nemade, P.K. Giri, Plasma-treated graphene surfaces for trace dye detection using surface-enhanced Raman spectroscopy, ACS Appl. Nano Mater. (2022), https://doi.org/10.1021/acsanm.2c00445 in press.
[26] G. Kalita, B.P. Jaisi, M. Umeno, Effective reduction and doping of graphene oxide films at near-room temperature by microwave-excited surface-wave plasma process, Diam. Relat. Mater. 126 (2022), 109066, https://doi.org/10.1016/j.diamond.2022.109066.
[27] Y. Lu, Y. Huang, M. Zhang, Y.J. Chen, Nitrogen-doped graphene materials for supercapacitor applications, Nanosci. Nanotechnol. 14 (2014) 1134–1144, https://doi.org/10.1166/jnn.2014.9102.
[28] H. Wang, T. Maiyalagan, X. Wang, Review on recent progress in nitrogen-doped graphene: synthesis, characterization, and its potential applications, ACS Catal. 2 (2012) 781–794, https://doi.org/10.1021/cs200652y.
[29] Y.-B. Tang, L.-C. Yin, Y. Yang, X.-H. Bo, Y.-L. Cao, H.-E. Wang, W.-J. Zhang, I. Bello, S.-T. Lee, H.-M. Cheng, C.-S. Lee, Tunable band gaps and p-type transport properties of boron-doped graphenes by controllable ion doping using reactive microwave plasma, ACS Nano 6 (2012) 1970, https://doi.org/10.1021/nn3005262. –8.
[30] N. McEvoy, H. Nolan, N.A. Kumar, T. Hallam, G.S. Duesberg, Functionalisation of graphene surfaces with downstream plasma treatments, Carbon 54 (2013) 283–290, https://doi.org/10.1016/j.carbon.2012.11.040.
[31] S.C. Hernández, F.J. Bezares, J.T. Robinson, J.D. Caldwell, S.G. Walton, Controlling the Local Chemical Reactivity of Graphene through Spatial Functionalization Carbon, vol. 60, 2013, pp. 84–93, https://doi.org/10.1016/j.carbon.2013.03.059.
[32] M. Scardamaglia, C. Struzzi, S. Osella, N. Reckinger, J.-F. Colomer, L. Petaccia, R. Snyders, D. Beljonne, C. Bittencourt, Tuning nitrogen species to control the charge carrier concentration in highly doped graphene, 2D Mater. 3 (2016), 011001, https://doi.org/10.1088/2053-1583/3/1/011001.
[33] H.M. Jeong, J.W. Lee, W.H. Shin, Y.J. Choi, H.J. Shin, J.K. Kang, J.W. Choi, Nitrogen-doped graphene for high-performance ultracapacitors and the importance of nitrogen-doped sites at basal planes, Nano Lett. 11 (2011) 2472–2477, https://doi.org/10.1021/nl2009058.
[34] Y. Zhu, S. Murali, M.D. Stoller, A. Velamakkani, R.D. Piner, R.S. Ruoff, Microwave assisted exfoliation and reduction of graphite oxide for ultracapacitors, Carbon 48 (2010) 2106–2122, https://doi.org/10.1016/j.carbon.2010.02.001.
[35] I. Bertóti, I. Mohai, M. Mohai, J. Szépvölgyi, Surface modification of multi-wall carbon nanotubes by nitrogen attachment, Diam. Relat. Mater. 20 (2011) 965–968, https://doi.org/10.1016/j.diamond.2011.05.011.
[36] J. Chen, X. Shi, S. Qi, M. Mohai, I. Bertóti, Y. Gao, H. Dong, Reducing and multiple-element doping of graphene oxide using active screen plasma treatments, Carbon 95 (2015) 338–346, https://doi.org/10.1016/j.carbon.2015.08.046.
[37] I. Bertóti, M. Mohai, K. László, Surface modification of graphene and graphite by nitrogen plasma: determination of chemical state alterations and assignments by quantitative X-ray photoelectron spectroscopy, Carbon 84 (2015) 185–196, https://doi.org/10.1016/j.carbon.2014.11.056.
[38] Y.F. Lu, S.T. Lo, J.C. Lin, W. Zhang, J.Y. Lu, F.H. Liu, C.M. Tseng, Y.H. Lee, C. Te Liang, L.J. Li, Nitrogen-doped graphene sheets grown by chemical vapor deposition: synthesis and influence of nitrogen impurities on carrier transport, ACS Nano 7 (2013) 6522–6532, https://doi.org/10.1021/nn402102y.
[39] A. Zabet-Khosousi, L. Zhao, L. Pálová, M.S. Hybertsen, D.R. Reichman, A. N. Pasupathy, G.W. Flynn, Segregation of sublattice domains in nitrogen-doped graphene, J. Am. Chem. Soc. 136 (2014) 1391–1397, https://doi.org/10.1021/ja408463g.
[40] N.A. Kumar, H. Nolan, N. McEvoy, E. Rezvani, R.L. Doyle, M.E.G. Lyons, G. S. Duesberg, Plasma-assisted simultaneous reduction and nitrogen doping of graphene oxide nanosheets, J. Mater. Chem. 1 (2013) 4431–4435, https://doi.org/10.1039/C3TA10337D.
[41] X. Wang, X. Li, L. Zhang, Y. Yoon, P.K. Weber, H. Wang, J. Guo, H. Dai, N-doping of graphene through electrothermal reactions with ammonia, Science 324 (2009) 768–771, https://doi.org/10.1126/science.1170335.
[42] J. Zhang, J. Zhang, F. He, J. Chen, D. Wang, M. Shichun, H.Y. Yang, Defect and doping co-engineered non-metal nanocarbon ORR electrocatalyst, Nano-Micro Lett. 13 (2021) 65, https://doi.org/10.1007/s40820-020-00579-y.
[43] D.C. Marcano, D.V. Kosynkin, J.M. Berlin, A. Sinitskii, Z. Sun, A. Slesarev, L. B. Alemany, W. Lu, J.M. Tour, Improved synthesis of graphene oxide, ACS Nano 4 (2010) 4806–4814, https://doi.org/10.1021/nn1006368.
[44] M.J. Fernández-Merino, L. Guardia, J.I. Paredes, S. Villar-Rodil, P. Solís-Fernández, A. Martínez-Alonso, J.M.D. Tascón, Vitamin C is an ideal substitute for hydrazine in the reduction of graphene oxide suspensions, J. Phys. Chem. C 114 (2010) 6426–6432, https://doi.org/10.1021/jp100603h.
[45] W.H. Bragg, W.L. Bragg, The reflexion of X-rays by crystals, Proc. Roy. Soc. Lond. A 88 (1913) 428–438, https://doi.org/10.1098/rspa.1913.0040.
[46] P. Scherrer, Bestimmung der Größe und der inneren Struktur von Kolloidteilchen mittels Röntgenstrahlen, Göttinger Nachrichten Math. Phys. 2 (1918) 98–100, https://doi.org/10.1007/978-3-662-33915-2_7.
[47] L.G. Cancado, K. Takai, T. Enoki, General equation for the determination of the crystallite size L_a of nanographite by Raman spectroscopy, Appl. Phys. Lett. 88 (2006), 163106, https://doi.org/10.1063/1.2196057.
[48] M. Mohai, XPS MultiQuant: multimodel XPS quantification software, Surf. Interface Anal. 36 (2004) 828–832, https://doi.org/10.1002/sia.1775.
[49] M. Mohai, I. Bertóti, Calculation of overlayer thickness on curved surfaces based on XPS intensities, Surf. Interface Anal. 36 (2004) 805–808, https://doi.org/10.1002/sia.1769.
[50] S. Evans, R.G. Pritchard, J.M. Thomas, Relative differential subshell photoionization cross-sections (MgKα) from lithium to uranium, J. Electron. Spectrosc. Relat. Phenom. 14 (1978) 341–358, https://doi.org/10.1007/978-3-662-33915-2_7.
[51] R.F. Reilman, A. Msezane, S.T. Manson, Relative intensities in photoelectron spectroscopy of atoms and molecules, J. Electron. Spectrosc. Relat. Phenom. 8 (1976) 389–394, https://doi.org/10.1016/0368-2048(76)80025-4.
[52] S. Park, J. An, I. Jung, R.D. Piner, S.J. An, X. Li, A. Velamakanni, R.S. Ruoff, Colloidal suspensions of highly reduced graphene oxide in a wide variety of organic solvents, Nano Lett. 9 (2009) 1593–1597, https://doi.org/10.1021/nl803798y.
[53] M.A. Pimenta, G. Dresselhaus, M.S. Dresselhaus, L.G. Cançado, A. Jorio, R. Saito, Studying disorder in graphite-based systems by Raman spectroscopy, Phys. Chem. Chem. Phys. 9 (2007) 1276–1290, https://doi.org/10.1039/B613962K.
[54] A. Cuesta, P. Dhamelincourt, J. Laureyns, A. Martínez-Alonso, J.M.D. Tascón, Raman microprobe studies on carbon materials, Carbon 32 (1994) 1523–1532, https://doi.org/10.1016/0008-6223(94)90148-1.
[55] S. Claramunt, A. Varea, D. López-Díaz, M.M. Velázquez, A. Cornet, A. Cirera, The importance of interbands on the interpretation of the Raman spectrum of graphene oxide, J. Phys. Chem. C 119 (2015) 10123–10129, https://doi.org/10.1021/acs.jpcc.5b01590.
[56] S. Vollebregt, R. Ishihara, F.D. Tichelaar, Y. Hou, C.I.M. Beenakker, Influence of the growth temperature on the first and second-order Raman band ratios and widths of carbon nanotubes and fibers, Carbon 50 (2012) 3542–3554, https://doi.org/10.1016/j.carbon.2012.03.026.
[57] A.C. Ferrari, J. Robertson, Interpretation of Raman spectra of disordered and amorphous carbon, Phys. Rev. B 61 (2000) 14095–14107, https://doi.org/10.1103/PhysRevB.61.14095.
[58] K.S. Kim, Y. Zhao, H. Jang, S.Y. Lee, J.M. Kim, K.S. Kim, J.-H. Ahn, P. Kim, J.-Y. Choi, B.H. Hong, Large-scale pattern growth of graphene films for stretchable transparent electrodes, Nature 457 (2009) 706–710, https://doi.org/10.1038/nature07719.
[59] I. Calizo, A.A. Balandin, W. Bao, F. Miao, C.N. Lau, Temperature dependence of the Raman spectra of graphene and graphene Multilayers, Nano Lett. 7 (2007) 2645, https://doi.org/10.1021/nl071033g. –9.
[60] L. Liu, S. Ryu, M.R. Tomasik, E. Stolyarova, N. Jung, M.S. Hybertsen, M. L. Steigerwald, L.E. Brus, G.W. Flynn, Graphene oxidation: thickness-dependent etching and strong chemical doping, Nano Lett. 8 (2008) 1965–1970, https://doi.org/10.1021/nl0808684.
[61] L.G. Cançado, K. Takai, T. Enoki, General equation for the determination of the crystallite size La of nanographite by Raman spectroscopy, Appl. Phys. Lett. 88 (2006), 163106, https://doi.org/10.1063/1.2196057.
[62] D. Yin, N. Lu, Z. Li, J. Yang, A computational infrared spectroscopic study of graphene oxide, J. Chem. Phys. 139 (2013), 084704, https://doi.org/10.1063/1.4818539.
[63] X. Jiao, Y. Qiu, L. Zhangab, X. Zhang, Comparison of the characteristic properties of reduced graphene oxides synthesized from natural graphites with different graphitization degrees, RSC Adv. 7 (2017) 52337–52344, https://doi.org/10.1039/C7RA10809E.
[64] J.L. Figueiredo, M.F.R. Pereira, M.M.A. Freitas, J.J.M. Orfao, Modification of the surface chemistry of activated carbons, Carbon 37 (1999) 1379–1389, https://doi.org/10.1016/S0008-6223(98)00333-9.
[65] D.I. Patel, D. Shah, S. Bahr, P. Dietrich, M. Meyer, A. Thißen, M.R. Linford, Water vapor, by near-ambient pressure XPS, Surf. Sci. Spectra 26 (1) (2019), 014026, https://doi.org/10.1116/1.5111634.
[66] G. Beamson, D. Briggs, High Resolution XPS of Organic Polymers – the Scienta ESCA300 Database, John Wiley and Sons, Chichester, 1992, p. 53.
[67] M. Mohai, K. László, I. Bertóti, Reduction and covalent modification of graphene-oxide by nitrogen in glow discharge plasma, Surf. Interface Anal. 50 (2018) 1207–1212, https://doi.org/10.1002/sia.6411, 2018.

[68] J.F. Ziegler, M.D. Ziegler, J.P. Biersack, Stopping and Range of Ions in Matter (SRIM-2013), Annapolis, MD, USA, 2013. http://www.SRIM.org.
[69] S.T. Senthilkumar, S.O. Park, J. Kim, S.M. Hwang, S.K. Kwak, Y. Kim, Seawater battery performance enhancement enabled by a defect/edge-rich, oxygen self-doped porous carbon electrocatalyst, J. Mater. Chem. 5 (2017) 14174–14181, https://doi.org/10.1039/C7TA03298F.
[70] J. Quílez-Bermejo, E. Morallon, D. Cazorla-Amorós, Metal-free heteroatom-doped carbon-based catalysts for ORR. a critical assessment about the role of heteroatoms, Carbon 165 (2020) 434–454, https://doi.org/10.1016/j.carbon.2020.04.068.